Journal of Civil Engineering
The Institution of Engineers, Bangladesh
Vol. CE 27, No. 2, 1999

STRESS-PATH DEPENDENT BEHAVIOUR OF MICACEOUS SAND

M. Bokhtair[1], A. Muqtadir[2], and M. H. Ali[2].

ABSTRACT : The behavior of micaceous sand depends on a number of factors including the mineralogical composition and the stress path followed during application of load. Although conventional triaxial compression (CTC) tests may be good enough for most of the cases, there are some applications such as retaining wall. excavation where the soil is subjected to shear stresses by gradual reduction of lateral pressure while vertical pressure remains essentially constant. This paper presents the results of an investigation carried on micaceous sands along the stress paths namely (i) hydrostatic compression ($\sigma_1 = \sigma_2 = \sigma_3$), (ii) conventional triaxial compression (σ_3 = constant), (iii) σ_1 = constant, and (iv) $\Delta\sigma_1 = \Delta\sigma_3$. Both elastic and plastic deformation obtained in hydrostatic compression increase with increasing mica content of the sands. It is observed that the angle of internal friction and initial tangent modulus depend on stress path followed during the tests. Axial strain and volumetric strain at failure also demonstrate stress path dependency.

INTRODUCTION

In most of the cases, conventional approach i.e. conventional triaxial compression test results are used to define stress-strain relationship of sand. However in some application such as retaining wall excavation of cuttings, the soil is subjected to shear stresses by progressive decrease of lateral pressure while the vertical stress remains essentially constant. In order to simulate the field conditions, it is necessary to perform the test on specimen along different stress paths. Use of different stress paths in the laboratory enable the field stress changes to be modeled more realistically than by using conventional tests alone.

Bell (1965) studied the behaviour of an Ottawa sand under hydrostatic stress and observed that the hydrostatic compression is nonlinear but almost elastic. Hydrostatic compression tests conducted by Ko and Scott (1967) on dense, medium dense and loose Ottawa

1 Department of Civil Engineering, B.I.T. Chittagong, Bangladesh
2 Department of Civil Engineering, BUET, Dhaka-1000, Bangladesh

sands show that the volumetric compression, ΔV varies nonlinearly with hydrostatic pressure, p and the relationship is of stiffening type. It was also found that the compressibility also depends on initial void ratio. El-Sohby and Andrawes (1972) reported that the compressibility of a granular material under hydrostatic pressure depends on the elastic properties of its individual particles.

Lade and Duncan (1976) reported that the strains induced by the changing stress from one state to another depend not only on the end points but also on the stress paths. The stress-strain-volume change relationships from tests along σ_3 constant, p_a constant and σ_1 constant stress paths on isotropically consolidated samples of Badarpur sand by Varadarjah and Mishra (1980) demonstrate stress path dependency. Hence, in order to obtain parameters corresponding to particular loading sequence in field, it becomes necessary to perform tests duplicating that stress path. Most of the above mentioned studies (Bell. 1965; ko and Scott, 1967; Lade and suncan, 1976) are essentially applicable for sand with little or without mica.

In many areas of Bangladesh, geotechnical engine have been encountered with sands containing significant amount of mica. They have to place the foundation on this sand. Opposing nature of frictional characteristics of mica and quartz and textural anomaly due to plate shape of mica particle necessitate the investigation involving them. At present, available study mainly concentrate on sand consist of quartz only. There is virtually no study regarding stress path dependency of micaceous sand. The present study focuses on the stress path dependency of micaceous sand.

Table 1. Physical properties of micaceous sands and density of the specimen

Sample Designation	Sample - Sl	Sample - S2	Sample - S3
Mica content (%)	2.50	4.00	6.00
Specific gravity	2.66	2.67	2.67
D_{10} (mm)	.31	.31	.31
D_{30} (mm)	.45	.45	.45
D_{60} (mm)	.91	.91	.91
Uniformity coefficient	2.93	2.93	2.93
Coefficient of curvature	0.72	0.72	0.72
Relative Density of the specimen (%)	29.0	63.0	85.0
Density State of the specimen	Loose	Medium Dense	Dense

EXPERIMENTAL PROGRAM

A number of specimen were tested along different compression stress paths. Initially, the specimen were subjected to an all-round pressure and then sheared along different stress paths by various combination of axial stress and cell pressure change. For tests along SP-C and SP-D, the axial streses were controlled by changing the dead load on the hanger. The hanger was placed on triaxial cell piston. The various combinations of axial stress and confining cell pressure produce the four compression stress paths as shown in Fig. 1. These are as follow :

SP-A: Hydrostatic compression ($\sigma_1 = \sigma_3$) test. This test was carried out by changing the confining cell pressure only. In this test, the specimen was subjected to an ambient cell pressure all along the test. This stress path includes loading and unloading–reloading cycles and finally a loading branch only.

SP-B: Conventional triaxial compression (σ_3 = constant) test. The specimen was failed by increasing the axial stress monotonically while the cell pressure, σ_3 was kept constant.

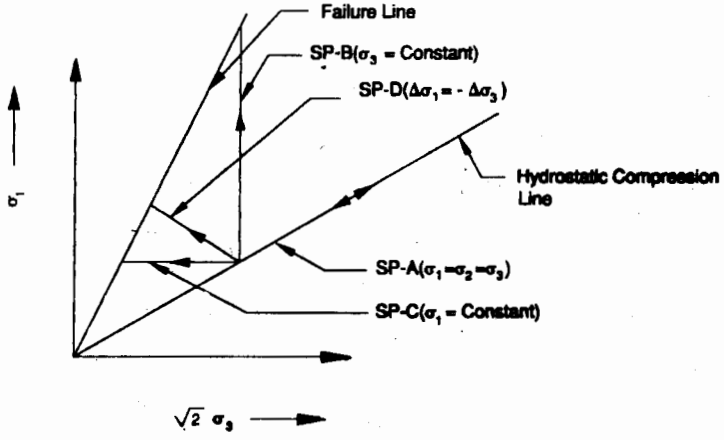

Fig 1. Stress Paths

SP-C: Major principle stress, σ_1 = constant test. The specimen was sheared to failure by keeping axial stress constant and decreasing the cell pressure. Reduction in axial stress, σ_1 resulting from decrease in cell pressure was compensated by adding dead load on the hanger.

SP-D: Triaxial compression test in which increase in σ_1 equals to decrease in minor principle stress, σ_3. Here the specimen was initially subjected to an all-round pressure. Then the shear stress in the specimen was introduced by increasing axial stress and reducing cell pressure such that the increment in axial stress equals to reduction in cell pressure. This process continued till the failure of the specimen occurred.

ANALYSIS AND INTERPRETATION OF RESULTS

Hydrostatic compression (SP-A)

The results of hydrostatic compression tests on Sample-S1, Sample-S2 and Sample-S3 are shown in Fig. 2. In this figure, the hydrostatic pressure is plotted against volumetric strain. An initial confining pressure or seating load of 30 kPa was applied to form the specimen and the volume change readings were observed for all pressures beyond this initial value. Figure 2 illustrates that the volumetric strain varies nonlinearly as the hydrostatic pressure and the relationship is of the stiffening type. For maximum pressure applied in these tests i.e. 455 kPa, no crushing of sand grain was observed. This is confirmed by comparing grain size distribution of samples before and after a test. The primary loading part of first cycle of curves, shown in Fig. 2, is similar to that reported by El-Sohby and Andrawes (1972). The loading-unloading curve of sample-S1 obtained in this investigation is similar to the findings of Ko and Scott (1967). Volumetric strains at various stages of hydrostatic compression of specimen are shown in Table-2. Table-2 demonstrates that, for all specimen, volumetric strains are not totally recovered after unloading. It is obseved that both elastic and plastic deformations increase with increasing mica content. This may be due to the higher compressibility and elastic property of the mica particles. For example, in case of sample-S1 at a hydrostatic pressure of 275 kPa, the volumetric strain during loading is 2.25% and volumetric strain during reloading is 2.60%. Such behaviour may be due to plastic deformation of the particle.

Triaxial compression tests along other stress paths

Drained triaxial compression tests are performed along different compression stress paths. Both stress controlled and strain controlled tests are performed. Deviator stress, axial strain and volumetric strain

are calculated from laboratory test data and these are plotted in the form of stress-strain-volumetric strain graphs.

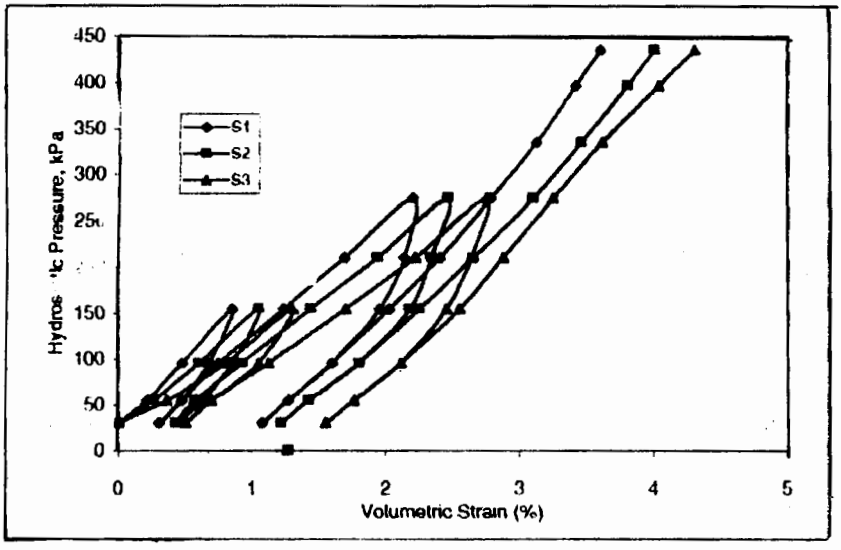

Fig 2. Results of Hydrostatic Compression, $\sigma_1 = \sigma_2 = \sigma_3$ Tests (SP-A)

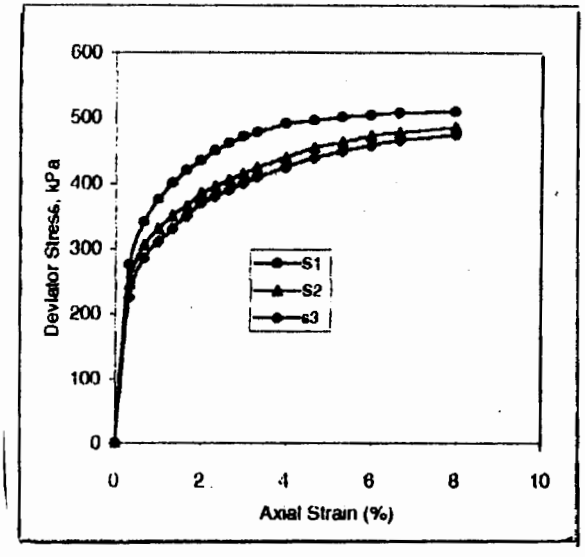

Fig 3a. Stress-Strain relationship of Samples S1, S2 and S3 in Conventional Triaxial σ_3 = Constant Tests (SP-B)

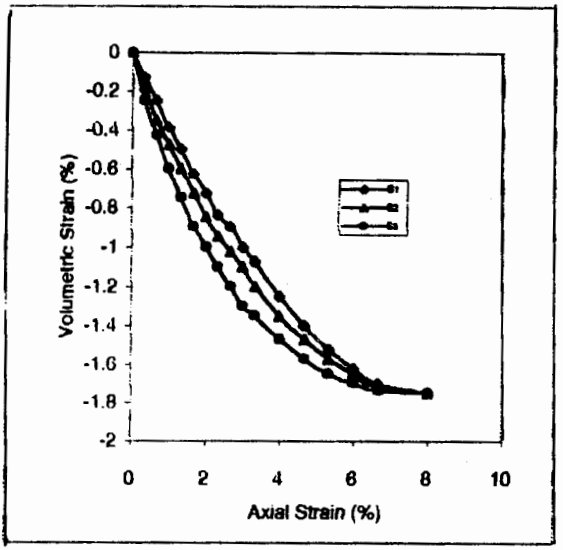

Fig 3b. Volume change-Strain relationship of Samples S1, S2 and S3 in Conventional Triaxial σ_3 = Constant Tests (SP-B)

Table 2. Volumetric Strain in Hydrostatic Compression

Sample Designation	Volumetric Strain (%)						
	1st Cycle			2nd Cycle			
	after Loading	After unloading	Elastic Deformation	After Loading	After Unloading	Elastic Deformation	Deformation at 455 kpa
S1	0.87	0.27	0.60	2.25	1.15	1.10	3.60
S2	1.06	0.41	0.64	2.50	1.25	1.25	4.00
S3	1.30	0.48	0.82	2.80	1.50	1.30	4.30

Conventional triaxial tests (SP-B):

The stress-strain-volume change diagrams obtained from triaxial tests along SP-B are shown in Fig. 3. During test of the specimen along this stress path, the mean effective principal stress increases. The relative density of the specimen prepared from Sample-S1, Sample-S2 and Sample-S3 are 29%, 63% and 85%, respectively. But these specimen give similar shape of stress-strain curves with no peak. This may be due to same initial void ratio of the specimen and higher compressibility of mica particles.

σ_1 = constant tests (SP-C):

Figure 4 represents the results obtained from tests along SP-C. In this test the axial stress was kept constant while radial stress reduced. This is a stress-controlled test. In this test the effective mean principal stress decreases. The specimen experienced deviator stress when the difference between axial and radial stress results from the reduction of radial stress. The test is performed for only one confining pressure. Confining pressure lower than 210 kPa could be used because of restriction imposed by self-weight of the loading frame. The stress-strain and volumetric strain vs volumetric axial strain curves have similar shape. The specimen undergo volumetric expansion from the beginning of the test. The axial strain and volumetric strain at failure increase with increasing mica content and failure stress for all samples are found to be independent of mica content.

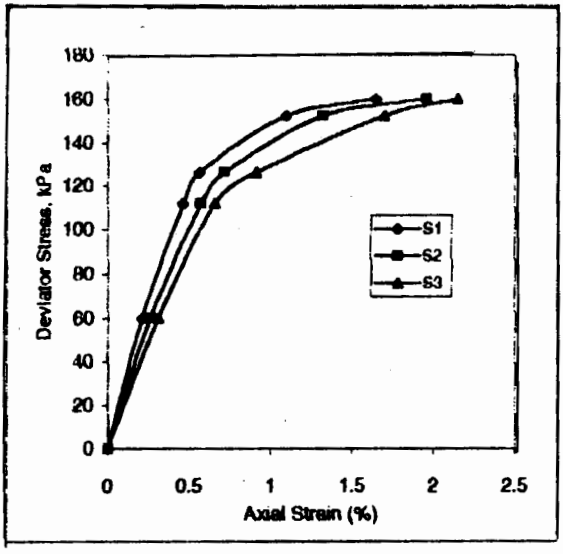

Fig 4a. Stress-Strain relationship of Samples S1, S2 and S3 in σ_1 = Constant Tests (SP-C)

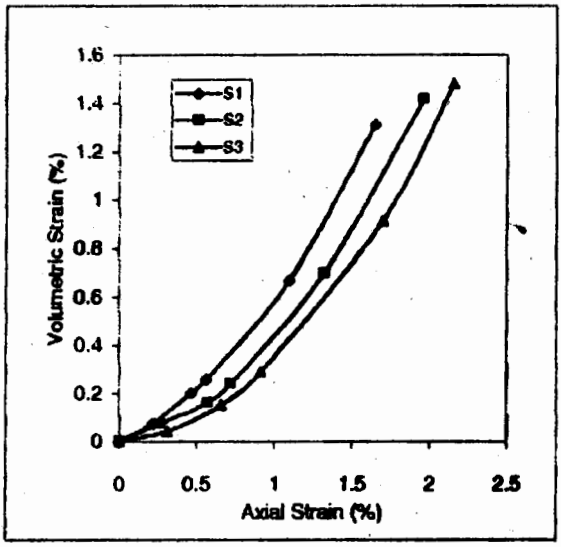

Fig 4b. Volume change-Strain relationship of Samples S1, S2 and S3 in σ_1 = Constant Tests (SP-C)

$\Delta\sigma_1$ = constant tests (SP-D):

Figure 5 shows the stress-strain-volume change curves obtained from triaxial compression test along SP-D. Shapes of these curves are similar. These tests were carried out controlling both axial stress and confining cell pressure. In these tests the axial stress is increased and the radial stress is decreased by an amount equal to the increment of axial stress. As a result, the effective mean principal stress reduces with progress of test. The volumetric strain is always expansive. At lower stress difference, the specimen undergo smaller amount of axial strain and volume change. But near failure, relatively smaller increase of deviator stress results in larger strain.

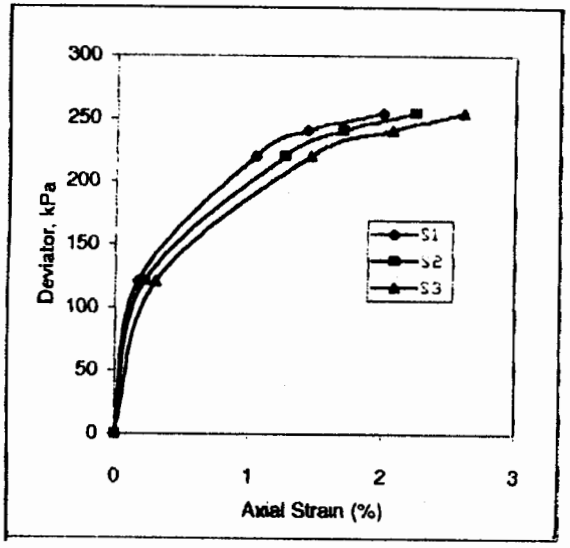

Fig 5a. Stress-Strain relationship of Samples S1, S2 and S3 in $\Delta\sigma_1 = \Delta\sigma_3$ Tests (SP-D)

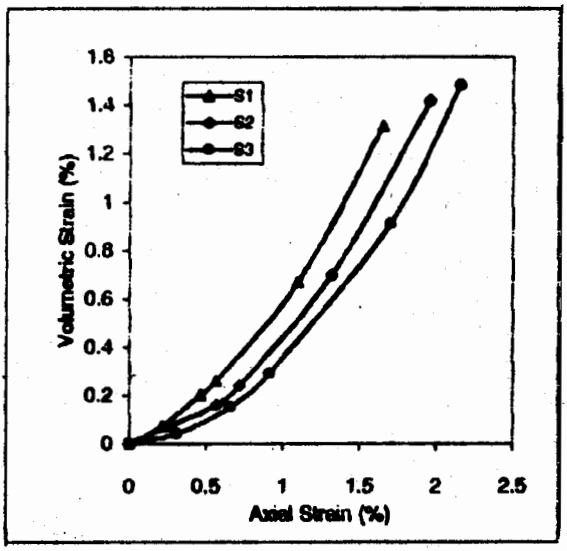

Fig 5b. Volume change-Strain relationship of Samples S1, S2 and S3 in $\Delta\sigma_1 = \Delta\sigma_3$ Tests (SP-D)

Effects of Stress Paths

Results of tests on specimen at an initial confining pressure of 210 kPa along different stress paths are used to examine the stress path dependency of the behaviour of micaceous sand. Tests along SP-C (σ_1 = constant) and SP-D ($\Delta\sigma_1 = \Delta\sigma_3$) were performed by controlling stress. Deviator stress on the specimen is introduced by various combination of axial and radial stress.

Table 3 illustrates the effect of stress path on the angle of shearing resistance. The table shows that the SP-C (σ_1= constant) has the largest angle of shearing resistance while SP-B (σ_3 = constant) has lowest angle of shearing resistance regardless of mica content. The angle of shearing resistance obtained from tests along SP-D is close to that of SP-C (σ_1= constant) and far away from that of SP-B (σ_3 = constant). Hence, it is seen that the stress path has influence on the angle of shearing resistance.

The effect of stress path on initial tangent modulus is represented in Table 4. The values presented in the table revealeds that stress path SP-B has largest value of tangent modulus and stress path SP-C has lowest value.

Table 5 shows the relationship between the stress path and axial strain at failure. Stress path SP-B shows the largest axial strain at failure and stress path SP-C indicate lowest value. Stress path SP-D shows values of axial strain which are very close to the value obtained from stress path SP-C. Varadarajan and Misra (1980) also reported similar results.

Table 3. Variation of Angle of Internal Friction with Stress Path for different Micaceous Sands

Sample Designation	Mica Content (%)	Angle of Internal Fricition		
		SP - B	SP - C	SP - D
S1	2.50	33.2	38.0	36.5
S2	4.00	32.4	38.0	36.5
S3	6.00	32.0	38.0	36.5

Table 4. Variation of Tangent Modulus with Stress Path for different Micaceous Sands

Sample Designation	Mica Content (%)	Initial Tangent Modulus, kpa		
		SP - B	SP - C	SP - D
S1	2.50	75000	34000	42000
S2	4.00	66000	28000	39000
S3	6.00	59000	24000	37000

Table 5. Variation of Axial Strain with Stress Path for different Micaceous Sands

Sample Designation	Mica Content (%)	Axial Strain at Faliure (%)		
		SP - B	SP - C	SP - D
S1	2.50	8.00	1.65	2.00
S2	4.00	8.00	1.98	2.25
S3	6.00	8.00	2.15	2.60

Table 6. Variation of Volumetric Strain with Stress Path for different Micaceous Sands

Sample Designation	Mica Content (%)	Volumatric Strain at Failure (%)		
		SP - B	SP - C	SP - D
S1	2.50	-1.75	1.30	0.80
S2	4.00	-1.75	1.41	0.91
S3	6.00	-1.75	1.47	1.01

The volumetric strains obtained from tests performed at a confining pressure are listed in Table 6. For stress paths SP-B, the volumetric strains are entirely compressive while for other two stress paths the dilation of the specimen begins from the commencement of test and continue till failure occur. Similar behaviour has also been noted by Krishnamurthy et al. (1981). Stress path SP-D gives smaller volumetric strain as stress path SP-C.

SUMMARY AND CONCLUSIONS

A series of hydrostatic compression tests and another series of triaxial compression tests along different stress paths were performed

on micaceous sands containing various percentages of mica. Hydrostatic compression tests were conducted to obtain behaviour of these sands under isotropic consolidation. Results of triaxial compression tests were used to detect stress path dependency of the micaceous sands. It is observed that the deformation in hydrostatic compression depends on mica content of the specimen. The volumetric compression increases with increasing mica content. Loading history also influence the behaviour of sands under hydrostatic compression.

For all stress paths used in this study, specimen were initially subjected to a hydrostatic pressure of 210 kPa and the deviator stresses were then applied by changing σ_1 and σ_3. Although the initial confining pressure for all stress paths were same, at failure confining pressure differed from each other depending on the stress paths followed. For SP-B, the confining pressure at failure was 210 kPa, while deviator stress about 500 kPa. In case of SP-C, the radial and axial pressures were 50 kPa and 160 kPa, respectively and for SP-D, these were 85 kPa and 250 kPa, respectively. Stress-strain diagrams obtained from tests along these stress paths illustrate that an increasing confining pressure has three effects: it reduces brittle characteristics of the stress-strain curve, it increases the axial strain at failure, and it decreases tendency to dilate. Hence it may be concluded that stress path dependency is due to variation in confining pressure at failure. This shows that the conventional triaxial tests may be used to determine parameter for other stress paths if the confining pressure at failure is previously known.

REFERENCES

Bell, J. M. (1965), "Stress-strain characteristics of cohesionless granular materials subjected to statically applied homogeneous loads in an open system", Ph. D. Thesis, California Institute of Technology, Pasadena, California, USA.

Bokhtair, M. (1993), "Stress path dependent stress-strain behaviour of micaceous sands," M. Sc. Thesis, Dept. of Civil Engg. University of Engineering and Technology, Dhaka, Bangladesh.

El-Sohby, M.A. Andrawes, K.Z. (1972), "Deformation characteristics of granular materials under hydrostatic compression," Canadian Geotechnical Journal, Vol. 9, 338.

Ko, H. Y. and Scott, R. F. (1967), "Deformation of sand in hydrostatic compression," Journal of Soil Mechanics and Foundation Engineering Division, ASCE, Vol 93, No. SM3, Proc. Paper 5245. pp. 137 ñ 153.

Krishnamurthy, M., Nagraj T. S. and Sridharan, A. (1981), "Stress path effects on the dilatant behavior of sand," Geotechnical Engineering, Vol. 12.

Lade, P.V. and Duncan, J. M. (1976), "Stress-path dependent behavior of cohesionless soil," Journal of Geotechnical Division, ASCE, Vol, 102, GTI. Proc. Paper 11841, Jan, 1976, pp 51 ñ 68.

Varadahrajan, A. and Mishra, S. S. (1980), "Stress-path dependent stress-strain-volume change behavior of a granular soil," Proceeding of International symposium on soils under cyclic and transient loading, Swansea.